IEEE Robotics and Automation Letters (RAL) paper presented at the
2020 IEEE International Conference on Robotics and Automation (ICRA)
31 May - 31 August, 2020. Paris, France

# Design of an Inflatable Wrinkle Actuator with Fast Inflation/Deflation Responses for Wearable Suits

Junghoon Park, Junhwan Choi, Sangjoon J. Kim, Kap-Ho Seo, and Jung Kim*, *Member, IEEE*

***Abstract*— In recent years, inflatable actuators have been widely used in wearable suits to assist humans who need help in moving their joints. Despite their lightweight and simple structure, they have long inflation and deflation times, which make their quick use difficult. To resolve this issue, we propose an inflatable wrinkle actuator with fast inflation and deflation responses. First, a theoretical model is proposed to develop an actuator that satisfies the design requirements: the desired assistive torque and the foam factor based on the wearability. Second, we reduce the inflation and deflation times by partially controlling the actuator layers and by designing pneumatic circuits using a vacuum ejector. To validate the usability of the actuator in wearable suits, we applied it to a wearable knee suit, and the inflation and deflation times were 0.40 s and 0.16 s, respectively. As a result, we ensured that the actuator did not interfere with human knee joint movement during walking by creating any residual resistance.**

## I. Introduction

A number of wearable robots have been recently developed to assist humans who need help in joint movement [1], [2]. Most of these robots have hard structures to deliver accurate assistive forces to humans, but these hard structures can be dangerous and add considerable weight to the users. Therefore, soft wearable robots have been developed to prevent such problems [3]–[8]. Soft robots are lightweight and guarantee safe physical human–robot interactions [9].

Typically, soft wearable suits have four types of actuators. The first type of actuator is the pneumatic muscle actuator (PMA), and most soft wearable suits have been developed using PMAs [10]–[12]. Although PMAs are lightweight with compliant structures and can generate a large force, they have a limited stroke length, which can place constraints on the user's natural motion. The second type of actuator uses a cable-driven mechanism, which has a higher bandwidth than other actuators; however, delivering comfortable and controlled assistance is difficult [13]–[15]. The third type of actuator used for suits is the elastomeric actuator [16]–[18], in which the elastic strain helps eject the air during depressurization, and the movement of the actuator can be predicted based on the mechanism geometry. Although air exhaust is easy to control, quantitatively designing and fabricating such actuators is difficult. In addition, they have insufficient mechanical power compared with other actuators. The fourth type of actuator is the inflatable actuator; these actuators have been recently developed and are lighter than other soft actuators, and their structure can be easily manufactured in various ways [7], [19]–[25]. An inflatable actuator can be designed based on a theoretical model to satisfy design requirements, such as the assistive torque requirement. The structure of the actuator can be manufactured without any constraints.

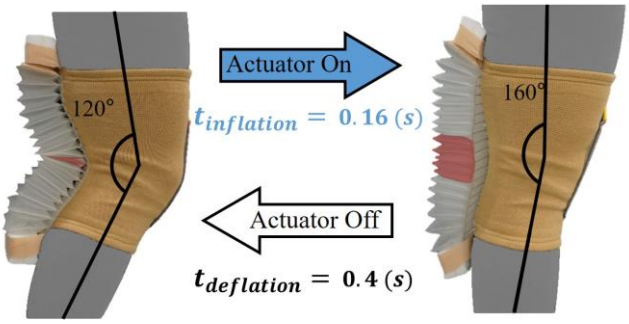


Fig. 1. Wearable knee suit with an inflatable wrinkle actuator to assist knee flexion and with fast inflation/deflation responses obtained via partial control of the wrinkle structure.

For the above reasons, inflatable actuators have been widely applied to wearable suits. Several types of wearable suits have been developed to assist in knee extensions during the swing phase of the gait cycle and during sit–stand motion [19-21], assist in ankle plantar flexion during walking [22], and assist in elbow flexion when lifting objects [23]. Although inflatable actuators can support human joints, the inflation and deflation responses have not been sufficiently analyzed in previous studies to improve the actuation speed. To assist various human joints, fast inflation and deflation responses are important to reduce the resistance that interferes with human movements. For example, if the air is not supplied and exhausted according to the gait cycle on time, then the user cannot bend his/her knee immediately after the stance phase and receive assistance during the swing phase.

In this paper, we proposed an inflatable wrinkle actuator with fast inflation and deflation responses for wearable robots, as shown in Fig. 1. The wrinkle structure can output a large torque relative to the same volume of other structures. The inflatable wrinkle actuator was designed based on the proposed theoretical model considering the desired assistive joint torque and actuator dimensions for the user's wearability. We partially controlled the actuator layers, improving the inflation and deflation responses compared to other inflatable wrinkle actuators. In addition, the deflation time was reduced by designing pneumatic circuits to momently create a negative pressure at the actuator outlet. Finally, we applied the

*Research supported by the ICT R&D program of MSIP/IITP. [2017-0-01724, Development of a soft wearable suit using intelligent information and meta-material/structure technology for fall prediction and prevention]

J. Park, J. Choi, S. J. Kim, and J. Kim are with the Dept. of Mechanical Engineering at KAIST, 291 Daehak-ro, Yuseong-gu, Daejeon 305-701, Republic of Korea (corresponding author to provide phone: 82-42-350-5230; email: jungkim@ kaist.ac.kr).

K. H. Seo is with the Disaster Robotics R&D Center, Korea Institute of Robot and Convergence, 30 Haean-ro, Heunghae-eup, Buk-gu, Pohang, Gyeongsangbuk-do, 37530, Republic of Korea (email: neoworld@kiro.re.kr)

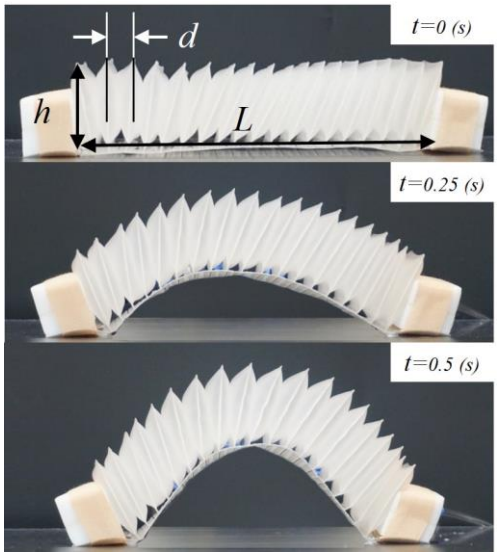


Fig. 2. An inflatable actuator before and after inflation with the dimension descriptions of the height of the layers ($h$), the distance between the layers ($d$), and the length ($L$) of the actuator.

developed actuator to a soft-knee suit to identify the possibility of application to wearable robotic systems. Section 2 introduces the fabrication of the actuator and the analytical model. In Section 3, we describe the validation of the model and the response analysis. Moreover, we introduce a knee-assisted system with the developed actuator. Using a walking experiment, we verify that the actuator can assist the human knee during walking. The conclusion is given in Section 4.

## II. Inflatable Actuator Design

### A. Fabrication

Fig. 2 shows the developed inflatable wrinkle actuator. The thermoplastic polyurethane (TPU) film (JTC1003, Jinheung Industry Co., Ltd, South Korea) was sealed using high-frequency welding, which utilizes an electromagnetic field. The thickness of the TPU film was 0.3 mm, and the Shore hardness was 85 Hs; therefore, each layer was flexible similar to fabric. The total weight of the actuator was 102 g, and the diameter of the tube was 6 mm. Fig. 2 presents the developed inflatable actuator in deflated and inflated states with descriptions of the actuator dimensions. As shown in Fig. 3, two PU foam cubes were attached to the ends of the actuator layers to keep the layers perpendicular to the bottom plate and restore the shape after a large deformation. The user does not feel any inconvenience while sitting on a chair because the height of the cubes is reduced to less than 2 mm during deformation. After the user stands up, the shape of the cubes is immediately restored. To inflate the actuator, air is flowed into one end of the actuator, and this air is supplied to the non-operated layers, as shown in Fig. 3. The three red middle layers, called the operated layers, are separately controlled from the rest of the layers. During the operation of the actuator, air enters or exits from the middle three layers to ensure the movement of human joints.

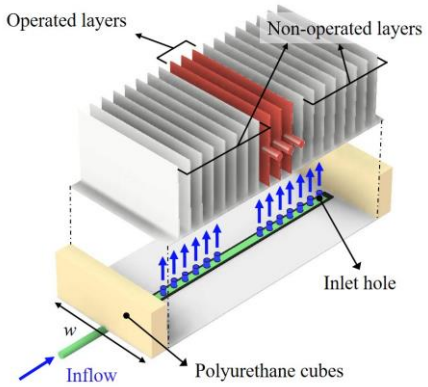


Fig. 3. Graphical illustration of the inflatable actuator: the non-operated layers are inflated through inlet holes connected to one inlet port (see blue arrows). Two polyurethane cubes are attached to both ends of the actuator to support the layers.

### B. Theoretical design

A theoretical model was constructed to analyze the kinematic response of the inflatable actuator after pressurization. We designed the inflatable actuator to assist the knee torque. According to the literature, the peak torque generated during the swing phase of the leg is 0.2 Nm/kg at a walking speed of 1.25 m/s, with a maximum knee angle of 120°; the torque generated during the stance phase is 0.4 Nm/kg, with a maximum knee angle of 160° [26]. We decided to assist the knee joint in performing normal walking; therefore, 100% assistance was set as the required torque to be provided to the knee joint during the swing phase for a person weighing 70 kg [27]. The design parameters were defined before designing the inflatable actuator. As shown in Figs. 2 and 3, the design parameters to be defined were the width ($w$), length ($L$), interval length between each layer ($d$), and height ($h$) of the inflatable actuator. Initially, the width ($w$) was set at 100 mm based on the breadth of a male subject's knee [28]. The length of the actuator ($L$) was chosen as 200 mm based on a previously developed inflatable actuator for a soft-knee exosuit [19]. Therefore, the parameters to be decided were the height of the layers ($h$) and the interval length between each layer ($d$).

As air is supplied to each layer of the inflatable actuator, each layer pushes against its adjacent layers, causing the actuator to bend, and the actuator applies the force to the human leg linkages. When two layers expand, they create a contact surface between the layers, as shown in Fig. 4 (a). As the air pack expands, a force is applied to the area of the contact surface under pressure. In Fig. 4 (a), the bending angle ($\theta$) is the same as the knee angle, and $L$ is the length of the actuator. The radius of curvature ($R$) of the inflatable actuator is given as

$$R = \frac{L}{\theta}, \tag{1}$$

and the angle between the two layers ($\theta'$) is defined as

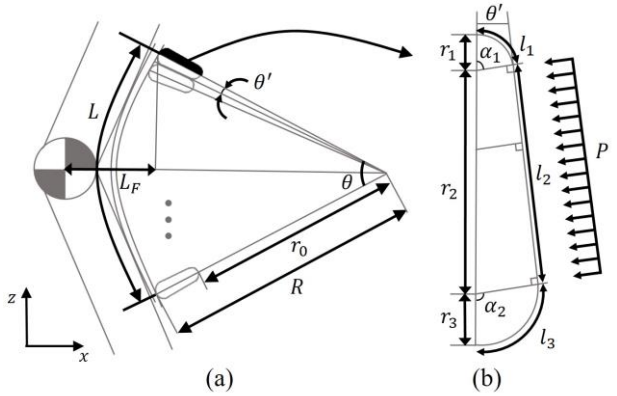


Fig. 4. (a) Geometric representation of the actuator in the inflated state demonstrating interactions among the layers. (b) Cross section of an individual layer showing the dimensions of the theoretical model.

$$\theta' = \frac{\theta}{2(n-1)}, \tag{2}$$

where $n$ is the number of layers installed in the actuator. Fig. 4 (b) presents the cross section of an individual layer, showing the dimensions for calculating the interacting area. From Fig. 4 (b), $\theta'$ can be defined in another way:

$$\theta' = \frac{\pi}{2} - \alpha_1 = \alpha_2 - \frac{\pi}{2}, \tag{3}$$

The dimensions ($l_1$, $l_2$, and $l_3$) for calculating the interacting area are as follows:

$$\begin{bmatrix} l_1 \\ l_2 \\ l_3 \end{bmatrix} = \begin{bmatrix} r_1\alpha_1 \\ r_2 \sin\alpha_1 \\ r_3\alpha_2 \end{bmatrix} = \begin{bmatrix} r_1(\frac{\pi}{2} - \theta') \\ r_2 \cos\theta' \\ r_3(\frac{\pi}{2} + \theta') \end{bmatrix}, \tag{4}$$

The radius of curvature ($R$) of the inflatable actuator is the sum of $r_0$, $r_1$, $r_2$, and $r_3$:

$$R = r_0 + r_1 + r_2 + r_3, \tag{5}$$

where $r_0$ is the distance between the center of the actuator curvature and the end of the layer, as shown in Fig. 4 (a). In addition, $r_1$ and $r_3$ can be defined using $r_0$ as

$$r_1 = (r_0 + r_1)\sin\theta', \; r_3 = (r_0 + r_1 + r_2)\sin\theta', \tag{6}$$

Combining (5) and (6), $r_1$, $r_2$, and $r_3$ can be expressed by using $R$, $r_0$, and $\theta'$ as

$$\begin{bmatrix} r_1 \\ r_2 \\ r_3 \end{bmatrix} = \begin{bmatrix} \frac{\sin\theta'}{1-\sin\theta'} r_0 \\ \frac{1}{1+\sin\theta'} R - \frac{1}{1-\sin\theta'} r_0 \\ \frac{\sin\theta'}{1+\sin\theta'} R \end{bmatrix}, \tag{7}$$

The total outside area of each layer before and after expansion must be constant because each layer does not stretch with the TPU material. The total outside area ($S$) can be presented as

$$\begin{aligned} S &= 2wh = 2w(l_1 + l_2 + l_3) + 2A_{side} \\ &= 2w(l_1 + l_2 + l_3) + 2(r_1^2\alpha_1 + r_3^2\alpha_2 + (r_1 + r_3)l_2) \end{aligned}, \tag{8}$$

where the knee breadth $w$ is 100 mm. Substituting (4) and (7) into (8) and summarizing for $r_0$, we obtain

$$\begin{aligned} &(a-1)\{(a-1)(\frac{\pi}{2} - \theta') - a\cos\theta'\}r_0^2 \\ &+\left[ w\{(a-1)(\frac{\pi}{2} - \theta') - a\cos\theta'\} + (2ab - a - b)R\cos\theta' \right] r_0 \\ &+(1-b)\{(1-b)(\frac{\pi}{2} + \theta') + b\cos\theta'\}R^2 \\ &+\{(1-b)(\frac{\pi}{2} + \theta') + b\cos\theta'\}wR - wh = 0 \end{aligned}, \tag{9}$$

where $a$ and $b$ are constants given by

$$a = \frac{1}{1-\sin\theta'}, b = \frac{1}{1+\sin\theta'}. \tag{10}$$

From (9), $r_0$ is a function of $R$, $w$, $\theta'$, and $h$; $R$ and $w$ are already defined. Since $\theta'$ is a function of $n$, $r_0$ is determined by $n$ and $h$.

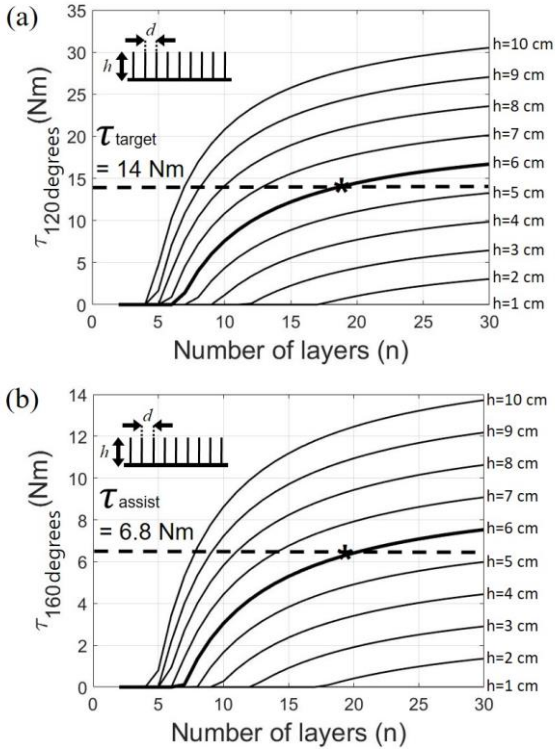


Fig. 5. (a) Torque at 120° estimated from the theoretical model for different numbers of layers ($n$) and heights of the layer ($h$). The black dotted line indicates the target torque generated by the inflatable actuator. (b) Torque at 160° estimated from the theoretical model for different numbers of layers ($n$) and heights of the layer ($h$). The black dotted line indicates the torque generated by the inflatable actuator.

The force is determined by the pressure within each layer and the contacting area between two layers as follows:

$$F = PA = Pwl_2 = Pwr_2 \cos\theta' = Pw(\frac{1}{1+\sin\theta'}R - \frac{1}{1-\sin\theta'}r_0)\cos\theta' \quad (11)$$

From (11), the force is a function of $n$ and $h$ because $\theta'$ and $r_0$ are related to $n$ and $h$. From Fig. 4 (a), the torque generated by the actuator on the two linkages is calculated as

$$T = FL_F, \quad (12)$$

where $L_F$ is the moment arm of the actuator considering the distance between the center of knee rotation and the back of the knee. Fig. 5 presents the torque from the actuator at 120° and 160° versus the number of layers ($n$) for different fixed values of $h$ at the maximum pressure of 50 $kPa$. We decided to provide 100% torque assistance to the knee joint for the swing phase (120° knee angle); therefore, the target torque was 14 Nm. As a result, the minimum height satisfying the target torque was 6 cm for 19 layers, as shown in Fig. 5 (a). With these dimensions, the actuator could assist 6.8 Nm at 160°, as shown in Fig. 5 (b).

## III. Experimental Results

### A. Experimental setup

In this section, we first validate the theoretical model by comparing the torque generated by the actuator with the torque estimated from the theoretical model. Then, we investigate the static response of the actuator deflation and inflation using a knee mock-up experimental setup. Fig. 6 (a) shows the experimental setup used to measure the torque; the setup consisted of a load cell (BCA-50L, CASKOEA Co., Ltd, South Korea) and an angle-adjustable 3D printed knee mock-up that mimics the human knee joint. The actuator was fixed behind the knee mock-up, and it generated a force on the load cell when the actuator expanded. Fig. 6 (b) presents the pneumatic circuit diagram used to reduce the deflation time of the actuator. The air supplied by the compressor (ECS 80G 4-213, EMG Elektromotorenwerk Grünhain, Germany) was controlled by a solenoid valve. Pressure gauges (PSE540-M5, SMC Co., Tokyo, Japan) measured the pressure at the inlet and outlet of the actuator, and the flow rate was measured by a flowmeter (PFM750S-C6-C, SMC Co., Japan). A vacuum ejector (ZU05SA, SMC Co., Japan) was used to create a negative pressure at the outlet of the actuator until the output valve was opened. After the valve was opened, the air was quickly released through the vacuum ejector because the pressure at the outlet of the actuator was lower than the atmospheric pressure.

### B. Torque measurement

Three inflatable actuators were inflated in increments of 10 kPa up to a maximum of 50 kPa during each of the three trials depending on the bending angle. The torque measured during a total of nine trials for each bending angle is plotted in Fig. 7. The developed actuator could generate 12.3 Nm (87.9% of knee torque) at a 120° bending angle and 6.2 Nm

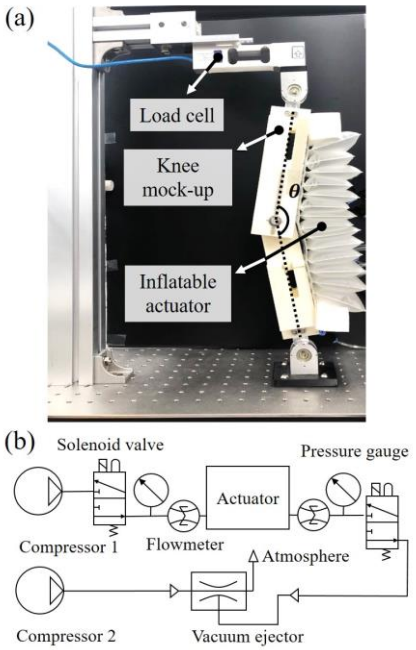


Fig. 6. (a) Experimental setup used to measure the torque generated by the actuator. (b) Pneumatic circuit diagram used to reduce the deflation time by using a vacuum ejector.

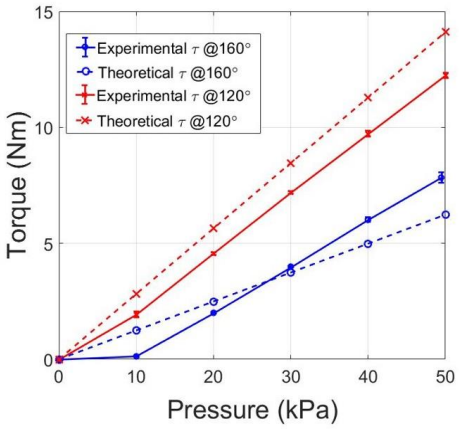


Fig. 7. Theoretically estimated torque versus experimentally measured torque.

(22.1% of knee torque) at a 160° bending angle. Compared with the theoretical model, the mean absolute percentage errors for the 120° and 160° bending angles were approximately 12.1% and 8.8%, respectively. Error occurred due to the deformation of the PU cubes installed at the ends of the actuator. When the force generated by the actuator was transmitted to the leg through the cubes, the radius of curvature ($R$) could change during the inflation of the actuator because of the deformation of the cubes. To reduce the error, the PU cubes can be replaced by another type of inflatable actuator or by a harder structure.

### C. Inflation - deflation response

Fast inflation and deflation responses are required to apply the actuator to wearable robots because slow responses impede the natural joint movements of humans. We targeted the knee as an auxiliary human joint; therefore, we first

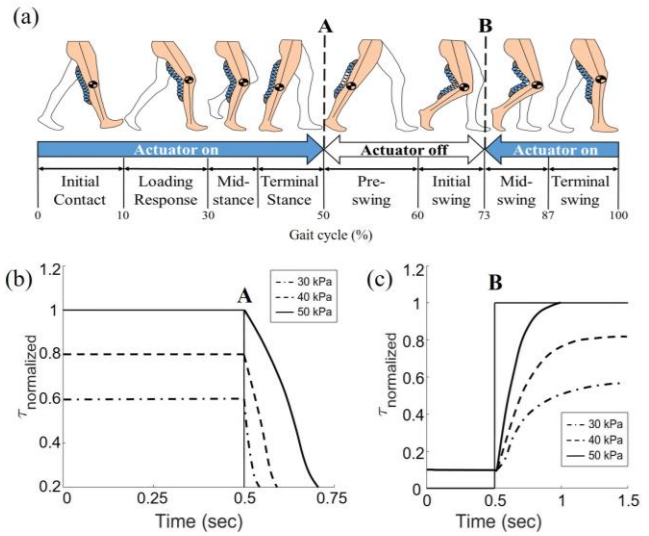


Fig. 8. (a) Actuator on and off periods according to the gait cycle. The actuator is deflated at point A and inflated at point B. (b) Deflation response of the actuator at point A for various pressures on all layers. (c) Inflation response of the actuator at point B to various input pressures on the operated layers, with 50 kPa filled in the non-operated layers.

investigated the human gait cycle. The gait cycle is largely separated into the stance and swing phases. In particular, the stance phase is divided into the following subphases: initial contact, loading response, mid-stance, and terminal stance. The swing phase is divided into pre-swing, initial swing, mid-swing, and terminal swing, as shown in Fig. 8 (a) [29]. The proposed actuator was developed to help the user stand on the ground during the stance phase and swing the leg forward during the swing phase. After the terminal stance, the knee is bent during the pre-swing and initial swing. In this period, the actuator is deflated so that residual resistance is not provided by the remaining air. Moreover, air should be supplied after the initial swing to help swing the leg from the mid-swing to loading response and support the leg during the single support phase, which is from the mid-stance to the terminal stance. A previous study showed that the average human walking speed is 1.25 m/s, and the cadence (i.e., the reciprocal of the stride duration) is 108.6 steps/min [30]. The total stride duration (i.e., the gait cycle) was calculated to be 0.52 s from the cadence. The duration from the pre-swing to the initial swing is 23% of the gait cycle, amounting to 0.12 s. This means that the air should be exhausted from the actuator within 0.12 s. The mid-swing to the terminal stance for the human gait takes 0.4 s (77% of the gait cycle), which means that air has to be supplied to the actuator within 0.4 s. Before validating the inflation and deflation responses of the actuator, we set the number of operated layers as three because the deflation response time increases as the number of operated layers increases, which makes simultaneously satisfying both the required deflation and inflation times difficult.

To investigate the deflation response of the actuator, the angle of the knee mock-up, shown in Fig. 6 (a), was set as 160° because the knee angle was 160° at the end of the terminal stance. All the layers of the actuator were inflated with 30, 40, and 50 kPa, and the air in the three middle operated layers was exhausted. As a result, the deflation response took up to 0.2 s for the 50 kPa case, as shown in Fig. 8 (b). The normalized torque ($\tau_{\text{normalized}}$) was the torque measured during the experiment divided by the maximum torque (12.3 Nm) measured at 160° in the previous section. In addition, we set the knee mock-up angle as 120° to mimic the human knee angle at the end of the initial swing (see point B in Fig. 8 (a)). Fig. 8 (c) shows the torque changes over the time taken to inject 30, 40, and 50 kPa of air into the three layers, with 50 kPa of air already injected into the non-operated layers. The results in Fig. 8 (c) show that filling the layers takes up to 0.5 s. We divided the measured torque by the maximum torque (6.2 Nm) measured at 120° to calculate the normalized torque. Because the actuator layers (with the exception of the operated layers) were filled with air, the remaining torque was generated by the actuator. Although the responses of the actuator did not perfectly meet the required times, they could be shortened when applying the actuator to a suit because a body weight is applied to the actuator, pressing the actuator. This will be discussed in the next section.

### *D. Knee exosuit validation*

We developed a knee exosuit using the developed actuator. The system was divided into three parts, as shown in Fig. 9. A portable pneumatic source supplied air to the actuator [31]. Fig. 9 (a) shows the portable pneumatic source and the master board. The master board (NI myRIO, National Instruments Co., USA) controlled the inlet and outlet solenoid valves (VQ110-6M-M5, SMC Co., Japan) based on the user's gait event measured by ground reaction force (GRF) sensors to control the actuator in real time. A custom 82-Wh battery powered the master board and the motor in the pneumatic source. As shown in Fig. 9 (b), the developed actuator was implemented behind the knee suit to assist the gait, and the inlet and outlet solenoid valves were installed at the side of the knee joint to not hinder the user's movement. The slave board measured the actuator pressure and the on/off states of two GRF sensors previously developed, which were installed in the toe and heel, as shown in Fig. 9 (c) [32], [33]. The gait phases were determined based on the on/off states of the GRF sensors, as shown in Fig. 10 (a). The phases were divided into two periods (actuator-on period and actuator-off period). The actuator-off period is from the pre-swing to the initial swing, and the actuator is deflated during this period. For the actuator-off period, the inlet solenoid valve is closed to block the transfer of air to the inflatable actuator, and the outlet valve is opened to enable the air within the actuator to freely exit to the atmosphere. From the mid-swing to the terminal stance, this period is called the actuator-on period, during which the actuator is inflated. During the actuator-on period, an assistive torque is generated by the actuator to help knee extension during the swing phase and to increase the stiffness during the stance phase. We designed a simple feedback bang-bang controller to generate a step input pressure profile, indicated as the blue dotted line in Fig. 10 (b). When the GRF sensor at the heel is lifted off the ground immediately after the terminal stance, the outlet valve is opened to release the air in the actuator to the atmosphere, and the inlet valve is closed at the same time. During the actuator-on period, the inlet solenoid valve is opened and the outlet solenoid valve is closed to

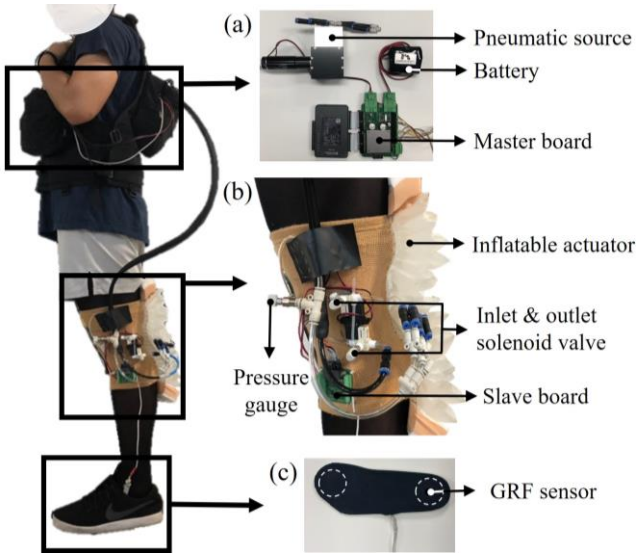


Fig. 9. Developed wearable knee suit. (a) Controller and pneumatic source inside the bag: air is supplied by the portable pneumatic power source, which is controlled by the master board. (b) Knee exosuit: air is controlled by the solenoid valves, and the pressure gauge measures the pressure in the actuator. (c) Ground reaction force (GRF) sensors: the user intention is detected by the insole-type GRF sensors embedded in the shoe.

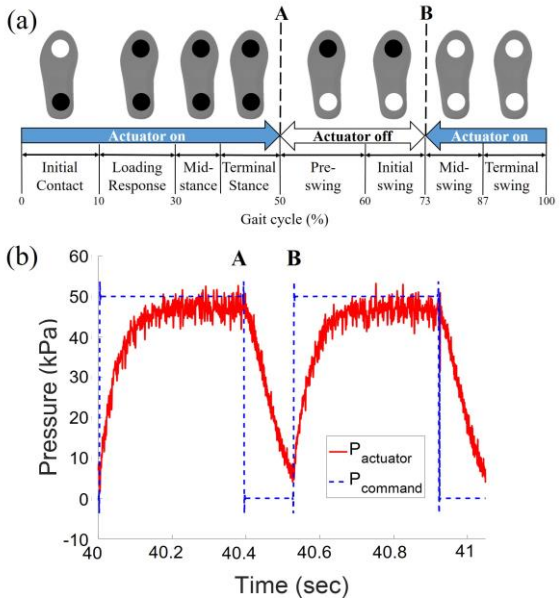


Fig. 10. (a) Actuator-on and -off periods according to the operation of the GRF sensors. (b) Pressure at the inlet of the actuator and command pressure generated by the controller according to the user intention during the walking test.

supply air to the actuator. The maximum supplied pressure in the actuator was set to 50 kPa.

The performance of the exosuit was evaluated using a healthy subject. In Fig. 10 (b), the blue dotted line shows the command pressure in the actuator. The command pressure was generated by the controller based on the gait cycle obtained in the walking test. From 40 to 40.4 s, air was supplied to the actuator until the internal pressure reached 50 kPa. On average, the air pressure reached 46 kPa in 0.4 s. The outlet solenoid valve was opened just before the swing phase started, which allowed the air to exhaust. We found that the air was exhausted from 47 to 6 kPa in 0.16 s. This means that air can be completely injected and exhausted from the actuator while walking. In addition, a user survey was conducted to investigate the comfort of the suit during the experiment. The subject replied that the actuator supported his leg by straightening his knee during the stance phase, and he properly felt the assistive force during the swing phase. Our results prove that the actuator can be applied to a wearable suit because it does not interfere with the user's movement.

## IV. Conclusion

In this study, we developed an inflatable wrinkle actuator for wearable suits that has quick inflation and deflation responses. By considering the size of the human joint, we proposed a theoretical model to satisfy the design requirements of the inflatable actuator, such as the desired assistive joint torque and the actuator dimensions. Using the theoretical model, we can design an actuator that produces the torque required to fit the joints that need to be assisted. Moreover, the exhaust structure of the actuator was modified, and a pneumatic circuit was designed to increase the deflation and inflation rates so that the speed was sufficient to not interfere with human joint movements. We applied the developed actuator to a wearable knee suit to validate the usability of the actuator in wearable suits. We confirmed that air can be discharged from and supplied to the actuator to facilitate the human gait cycle.

In our future work, first, we will improve the responses of the actuator. The actuator fabricated in this study was developed to assist the knee torque during normal walking at 1.25 km/h; for walking at higher speeds or running, faster inflation and deflation responses are required. To improve the responses, the layer volume would need to be reduced. As the volume of the layers is reduced, the thickness and Shore hardness of the TPU would need to be increased; otherwise, the layers will need to be coated by a fabric to withstand the high pressure [34]. Second, we will perform surface electromyography (sEMG) measurement of the lower limb muscles of the user to identify whether the developed wearable suit assists human joint motion. Finally, by using our inflatable actuator design method based on the theoretical model, we can extend the application of the developed actuator to various wearable suits, such as soft ankle orthosis or shoulder orthosis suits. For various applications, the durability of the actuator needs to be investigated. We propose to perform verification through modeling and by using the computational finite-element method to optimize the design parameters.

## Acknowledgment

This work was supported by the ICT R&D program of MSIP/IITP [2017-0-01724, Development of a soft wearable suit using intelligent information and meta-material/structure technology for fall prediction and prevention].

## REFERENCES


[1] T. Yan, M. Cempini, C. M. Oddo, and N. Vitiello, "Review of assistive strategies in powered lower-limb orthoses and exoskeletons," *Rob. Auton. Syst.*, vol. 64, pp. 120–136, Feb. 2015.

[2] R. A. R. C. Gopura, D. S. V. Bandara, K. Kiguchi, and G. K. I. Mann, "Developments in hardware systems of active upper-limb exoskeleton robots: A review," *Rob. Auton. Syst.*, vol. 75, pp. 203–220, Jan. 2016.

[3] A. T. Asbeck, S. M. M. De Rossi, I. Galiana, Y. Ding, and C. J. Walsh, "Stronger, Smarter, Softer: Next-Generation Wearable Robots," *IEEE Robot. Autom. Mag.*, vol. 21, no. 4, pp. 22–33, Dec. 2014.

[4] H. K. Yap *et al.*, "A Fully Fabric-Based Bidirectional Soft Robotic Glove for Assistance and Rehabilitation of Hand Impaired Patients," *IEEE Robot. Autom. Lett.*, vol. 2, no. 3, pp. 1383–1390, Jul. 2017.

[5] J. Kwon, J.-H. Park, S. Ku, Y. Jeong, N.-J. Paik, and Y.-L. Park, "A Soft Wearable Robotic Ankle-Foot-Orthosis for Post-Stroke Patients," *IEEE Robot. Autom. Lett.*, vol. 4, no. 3, pp. 2547–2552, Jul. 2019.

[6] C. Thakur, K. Ogawa, T. Tsuji, and Y. Kurita, "Soft Wearable Augmented Walking Suit With Pneumatic Gel Muscles and Stance Phase Detection System to Assist Gait," *IEEE Robot. Autom. Lett.*, vol. 3, no. 4, pp. 4257–4264, Oct. 2018.

[7] C. M. Thalman, Q. P. Lam, P. H. Nguyen, S. Sridar, and P. Polygerinos, "A Novel Soft Elbow Exosuit to Supplement Bicep Lifting Capacity," in *2018 IEEE/RSJ International Conference on Intelligent Robots and Systems (IROS)*, 2018, pp. 6965–6971.

[8] S.-H. Park, J. Yi, D. Kim, Y. Lee, H. S. Koo, and Y.-L. Park, "A Lightweight, Soft Wearable Sleeve for Rehabilitation of Forearm Pronation and Supination," in *2019 2nd IEEE International Conference on Soft Robotics (RoboSoft)*, 2019, pp. 636–641.

[9] D. G. CALDWELL, N. G. TSAGARAKIS, S. KOUSIDOU, N. COSTA, and I. SARAKOGLOU, "'SOFT' EXOSKELETONS FOR UPPER AND LOWER BODY REHABILITATION — DESIGN, CONTROL AND TESTING," *Int. J. Humanoid Robot.*, vol. 04, no. 03, pp. 549–573, Sep. 2007.

[10] Ching-Ping Chou and B. Hannaford, "Measurement and modeling of McKibben pneumatic artificial muscles," *IEEE Trans. Robot. Autom.*, vol. 12, no. 1, pp. 90–102, 1996.

[11] G. Andrikopoulos, G. Nikolakopoulos, and S. Manesis, "A Survey on applications of Pneumatic Artificial Muscles," in *2011 19th Mediterranean Conference on Control & Automation (MED)*, 2011, pp. 1439–1446.

[12] Y.-L. Park *et al.*, "Bio-inspired active soft orthotic device for ankle foot pathologies," in *2011 IEEE/RSJ International Conference on Intelligent Robots and Systems*, 2011, pp. 4488–4495.

[13] L. N. Awad *et al.*, "A soft robotic exosuit improves walking in patients after stroke," *Sci. Transl. Med.*, vol. 9, no. 400, p. eaai9084, Jul. 2017.

[14] A. T. Asbeck, S. M. M. De Rossi, K. G. Holt, and C. J. Walsh, "A biologically inspired soft exosuit for walking assistance," *Int. J. Rob. Res.*, vol. 34, no. 6, pp. 744–762, May 2015.

[15] A. T. Asbeck, K. Schmidt, and C. J. Walsh, "Soft exosuit for hip assistance," *Rob. Auton. Syst.*, vol. 73, pp. 102–110, Nov. 2015.

[16] Y.-L. Park, B. Chen, C. Majidi, R. J. Wood, R. Nagpal, and E. Goldfield, "Active modular elastomer sleeve for soft wearable assistance robots," in *2012 IEEE/RSJ International Conference on Intelligent Robots and Systems*, 2012, pp. 1595–1602.

[17] G. Agarwal, N. Besuchet, B. Audergon, and J. Paik, "Stretchable Materials for Robust Soft Actuators towards Assistive Wearable Devices," *Sci. Rep.*, vol. 6, no. 1, p. 34224, Sep. 2016.

[18] H. K. Yap, J. C. H. Goh, and R. C. H. Yeow, "Design and Characterization of Soft Actuator for Hand Rehabilitation Application," 2015, pp. 367–370.

[19] S. Sridar, Z. Qiao, N. Muthukrishnan, W. Zhang, and P. Polygerinos, "A Soft-Inflatable Exosuit for Knee Rehabilitation: Assisting Swing Phase During Walking," *Front. Robot. AI*, vol. 5, May 2018.

[20] S. Sridar, P. H. Nguyen, M. Zhu, Q. P. Lam, and P. Polygerinos, "Development of a soft-inflatable exosuit for knee rehabilitation," in *2017 IEEE/RSJ International Conference on Intelligent Robots and Systems (IROS)*, 2017, pp. 3722–3727.

[21] A. J. Veale, K. Staman, and H. van der Kooij, "Realizing Soft High Torque Actuators for Complete Assistance Wearable Robots," 2019, pp. 39–43.

[22] J. Chung, R. Heimgartner, C. T. Oneill, N. S. Phipps, and C. J. Walsh, "ExoBoot, a Soft Inflatable Robotic Boot to Assist Ankle During Walking: Design, Characterization and Preliminary Tests," in *2018 7th IEEE International Conference on Biomedical Robotics and Biomechatronics (Biorob)*, 2018, pp. 509–516.

[23] D. Govin, L. Saenz, G. Athanasaki, L. Snyder, and P. Polygerinos, "Design and Development of a Soft Robotic Back Orthosis," in *2018 Design of Medical Devices Conference*, 2018, p. V001T10A001.

[24] R. F. Natividad, M. R. Del Rosario, P. C. Y. Chen, and C.-H. Yeow, "A hybrid plastic-fabric soft bending actuator with reconfigurable bending profiles," in *2017 IEEE International Conference on Robotics and Automation (ICRA)*, 2017, pp. 6700–6705.

[25] W. Felt, "Folded-Tube Soft Pneumatic Actuators for Bending," *Soft Robot.*, vol. 6, no. 2, pp. 174–183, Apr. 2019.

[26] K. E. Zelik and A. D. Kuo, "Human walking isn't all hard work: evidence of soft tissue contributions to energy dissipation and return," *J. Exp. Biol.*, vol. 213, no. 24, pp. 4257–4264, Dec. 2010.

[27] wikipedia.org, "Human body weight," 2018. [Online]. Available: https://en.wikipedia.org/wiki/Human_body_weight. [Accessed: 11-Aug-2019].

[28] H.-J. Wilke, P. Neef, B. Hinz, H. Seidel, and L. Claes, "Intradiscal pressure together with anthropometric data – a data set for the validation of models," *Clin. Biomech.*, vol. 16, pp. S111–S126, Jan. 2001.

[29] J. Perry and J. Burnfield, *Gait Analysis: Normal and Pathological Function*. Thorofar, NJ: Slack, 1992.

[30] C. Kirtley, M. W. Whittle, and R. J. Jefferson, "Influence of walking speed on gait parameters," *J. Biomed. Eng.*, vol. 7, no. 4, pp. 282–288, Oct. 1985.

[31] S. J. Kim, H. Chang, J. Park, and J. Kim, "Design of a Portable Pneumatic Power Source With High Output Pressure for Wearable Robotic Applications," *IEEE Robot. Autom. Lett.*, vol. 3, no. 4, pp. 4351–4358, Oct. 2018.

[32] J. Park, S. Kim, Y. Na, Y. Kim, and J. Kim, "Development of a Bendable Outsole Biaxial Ground Reaction Force Measurement System," *Sensors*, vol. 19, no. 11, p. 2641, Jun. 2019.

[33] S. J. Kim, G. M. Gu, Y. Na, J. Park, Y. Kim, and J. Kim, "Wireless Ground Reaction Force Sensing System Using a Mechanically Decoupled Two-Dimensional Force Sensor," *IEEE/ASME Transactions on Mechatronics*, 2019.

[34] P. H. Nguyen, I. B. Imran Mohd, C. Sparks, F. L. Arellano, W. Zhang, and P. Polygerinos, "Fabric Soft Poly-Limbs for Physical Assistance of Daily Living Tasks," in *2019 International Conference on Robotics and Automation (ICRA)*, 2019, pp. 8429–8435.